X-722-74-301

PREPRINT

NASA TM X- 70863

MEASUREMENT OF THE LIDAR CROSS SECTIONS OF CUBE CORNER ARRAYS FOR LASER RANGING OF SATELLITES

P. O. MINOTT

SEPTEMBER 1974

GSFC

GODDARD SPACE FLIGHT CENTER

GREENBELT, MARYLAND

For information concerning availability
of this document contact:

Technical Information Division, Code 250
Goddard Space Flight Center
Greenbelt, Maryland 20771

(Telephone 301-982-4488)

X-722-74-301

MEASUREMENTS OF THE LIDAR CROSS SECTIONS OF CUBE CORNER ARRAYS FOR LASER RANGING OF SATELLITES

P. O. Minott

September 1974

GODDARD SPACE FLIGHT CENTER
Greenbelt, Maryland

CONTENTS

		Page
1.0	INTRODUCTION	1
2.0	SATELLITE COORDINATE SYSTEM	2
3.0	OPTICAL TESTING	2
4.0	POINT SPREAD FUNCTION	3
5.0	COMPUTATIONAL METHODS FOR DERIVING POINT SPREAD FUNCTION	4
6.0	EXPERIMENTAL POINT SPREAD FUNCTIONS	6
7.0	THE VELOCITY ABERRATION	8
8.0	EVALUATION CROSS SECTION	10
9.0	THE RADAR EQUATION	11

TABLES

Table		Page
1	Values of the Constant p For NASA Satellites	15
2	Maximum Velocity Aberration as a Function of Orbital Altitude	15
3	Variation of Apparent as a Function of Zenith Angle (θ) and Velocity Vector (ω) for Several Altitudes	16
4	Satellite Cross Section at Zenith	17

ILLUSTRATIONS

Figure		Page
1	. . . . .	18
2a	Optical Schematic of Test Setup for Measuring Cube Array Area.	19
2b	Optical Schematic of Test Setup for Measuring Point Spread Function.	20
3	Relative Area of GEOS A Cube Corner Panels as a Function of Incidence Angle	21
4	Far Field Patterns for Cube Corners Used on Several Satellites	22
5	Coordinate System for Far-Field Intensity Pattern	23
6	Definition of Parameters Used in Calculation of Velocity Aberration	24
7	Maximum Velocity Aberration as a Function of Orbital Altitude	25

1.0 INTRODUCTION

Over the past twelve years since 1964, I have been called upon to perform tests to determine the radar (lidar) cross section of several satellite retrodirector arrays used in conjunction with laser ranging experiments performed by NASA. These satellites have included BE-B, BE-C, GEOS I(A), GEOS II(B), GEOS III(C) and TIMATION III. As a result of this testing I have become familiar with many of the problems of designing and testing cube corner arrays. Much of the theory behind these tests has not previously been published. I have therefore collected many of my notes and assembled them into this document for the reader interested in cube corner array performance and testing. It is hoped that this paper will explain many of the questions left unanswered in a previous paper, "Design of Retrodirector Arrays for Laser Ranging of Satellites," X-723-74-122. This previous paper was intended as an introduction to cube corner array design and discussed arrays made up of diffraction limited cube corners. In practice the diffraction limit is seldom obtained due to manufacturing problems. Therefore in dealing with most arrays we have a more difficult problem in determining areas and gain functions.

The paper starts with section describing the satellite coordinate system necessary to describe the location and orientation of each cube corner in the array. The second section describes the method of optical testing. This is followed by sections defining the gain function, computational methods for deriving the gain function and experimental values for it. The velocity aberration is derived as a function of satellite orbit, a complete method for cross section evaluation is described, and finally the radar equation is described.

The methods used in this paper are analytical and do not employ computer techniques. This approach has the advatage of giving good insight into the problem. However, a computerized analysis is required to perform complete analysis. Several computer methods have been utilized by various authors with varying degrees of success, but, none of their programs have been documented nor are any of the methods capable of accounting for manufacturing errors. The author is presently working on a computerized analysis technique for cube arrays which will be partly based on previous programs, but will extend the analysis to include all of the effects described in this paper.

2.0 SATELLITE COORDINATE SYSTEM

Most of the satellites used for laser ranging targets to date have been either gravity gradient or otherwise stabilized so that one axis of the satellite remains constantly pointed at the earths center. For a laser tracking mission it is desirable to have the lidar cross section independent of the azimuth angle of the satellite viewed from the tracking station. Therefore the retro-director array is normally made as nearly as possible, a surface of revolution with constant cross section for all azimuth aspects. Before continuing in the discussion of retrodirector arrays, we must set up a definition of our frame of reference.

The position and orientation of cube corners in an array are normally specified in a spherical coordinate system with a polar axis defined by the line between the center of gravity of the spacecraft and the center of the earth as shown in Figure 1. The zero reference for the polar angle θ is the nadir of the satellite, and azimuth angles when required are defined relative to the velocity vector of the satellite with azimuth angles increasing in a counter-clockwise direction when viewed from earth. If the satellite spins about the polar axis, an arbitrary azimuth direction related to the structure of the satellite must be selected and a time relationship between this azimuth and the velocity vector established. However, in the case of spinning satellites, the designer normally makes the array rotationally symmetric so that the cross section becomes a function of polar angle θ alone. In the most general case, a cube corner location may be specified by three position coordinates (R_c, θ_c, ϕ_c) and two orientation coordinates (θ_n, ϕ_n) which specify the direction of the outward normal from the prism entrance pupil. The direction of the incident laser radiation may be specified by two angles with respect to the satellite coordinate system (θ_1, ϕ_1).

3.0 OPTICAL TESTING

In testing a satellite retrodirector array, we must determine the effective reflective area, and the gain as a function of the incident laser radiation coordinates. This is normally done as shown in Figure 2. The array is placed in the beam of an autocollimator and the total energy reflected from the array is compared to the energy reflected from a flat of known area and reflectivity. From this measurement we can calculate the effective area of the array. It should be pointed out that the optical losses in the cube corners are taken into account in this measurement method, and therefore no further efficiency corrections are necessary. The second part of our test is to scan the retrodirected intensity pattern in the collimator focal plane to determine the far field point spread function. This is normally done with a pinhole on an XY coordinate stage mounted in the collimator focal plane. Radiation passing

through the pinhole is detected by a photomultiplier. Both of these tests must obviously be done for all possible values of θ_1 and in the case of arrays which are not azimuthally symmetric for all ϕ_1. Examples of the results of the reflective area and for field pattern tests are shown in Figures 3 and 4.

4.0 POINT SPREAD FUNCTION

We can compute the lidar cross section in the following manner. The far field pattern is examined and an equation for intensity derived for it (Fig. 5)

$$I(\psi, \eta) = HA_e P(\psi, \eta) \tag{1}$$

where H is the incident irradiance, A_e is the effective area and $P(\psi, \eta)$ is the point spread function which describes the relative intensities in the far field. Since energy must be conserved

$$HA_e = \int_0^{2\pi} \int_0^{\infty} I(\psi, \eta)\, \psi d\psi d\eta$$

$$= HA_e \int_0^{2\pi} \int_0^{\infty} P(\psi, \eta)\, \psi d\psi d\eta \tag{2}$$

Therefore the definite integral must equal unity. The definition of cross section is

$$\sigma(\psi, \eta) = 4\pi \left[\frac{I(\psi, \eta)}{H}\right] \tag{3}$$

Substituting equation 1 into 3 we obtain

$$\sigma(\psi, \eta) = 4\pi \left[\frac{HA_e P(\psi, \eta)}{H}\right] = 4\pi A_e P(\psi, \eta) = G(\psi, \eta)\, A_e \tag{4}$$

Note that H, the irradiance has dropped out of the equation so that in our measurements it is not necessary to maintain a calibration of the irradiance level.

In making the photomultiplier scans of the far field patterns, there are many unknown experimental parameters which make it difficult to measure absolute values of intensity. Therefore relative intensities are plotted to an arbitrary ordinate determined by the experimental parameters. The intensities are then normalized by dividing their values by the ordinate at the (0, 0) position of the far field. From these curves, a suitable point spread function $P(\psi, \eta)$ must be inferred.

5.0 COMPUTATIONAL METHODS FOR DERIVING THE POINT SPREAD FUNCTION

The most obvious method for deriving the point spread function $P(\psi, \eta)$ would be to obtain the Fraunhofer diffraction pattern from the two dimensional Fourier transforms of the cube corners in the array. The point spread function could then be obtained by summing the amplitudes, squaring the sum and taking the absolute value. The result would be proportional to intensity and we could obtain $P(\psi, \eta)$ by a suitable normalization constant.

This has been done for an equilateral hexagon aperture by Smith and Marsh* who obtain the following relation

$$\frac{I}{I_0} = \left| \frac{1}{x^2} \left[\sin \nu_+ \frac{\sin \mu_-}{\mu_-} + \sin \nu_- \frac{\sin \mu_+}{\mu_+} \right] \right| \qquad (5)$$

where

$$k = 2\pi/\lambda$$

$$X = k\ell$$

$$Y = km$$

$$\mu_\pm = X/3 \pm Y\sqrt{3}$$

$$\nu_\pm = X \pm 2Y/\sqrt{3}$$

and ℓ and m are the tangents of the rectilinear angles in the far field which for small angles are equal to angles themselves.

*R.C. Smith and James C. Marsh, Journ. Opt. Soc. Am. 64, p. 798, June 1974.

The comparison of this equation against the measured intensity profiles shown in Figure 4 clearly indicates that this does not provide a satisfactory explanation of the actual intensity profiles.

In order to explain the actual patterns we must take the random manufacturing errors into account. From "The Scattering of Electromagnetic Waves from Rough Surfaces" by P. Beckmann and A. Spizzichino (Mac Millan 1963) we can treat the cube corner as a rough surface at normal incidence with the following equation

$$\langle \rho\rho^* \rangle = e^{-g} \left[\rho_0^2 + \frac{\pi T^2 F}{A} \exp\left(- \frac{\nu_{xy}^2 T^2}{4} \right) \right] \qquad (6)$$

where

$\langle \rho\rho^* \rangle$ = Ratio of mean scattered power in the direction specified divided by the power in the specular direction for a perfectly flat surface i.e. $I(\psi, \eta)/I_0$ (p. 29)*

$g = \left[\frac{2\pi\sigma}{\lambda}\right]^2 = k^2 \sigma^2$ for normal incidence (p. 82)*

ρ_0^2 = Fraunhofer diffraction term (p. 82)*

T = Correlation distance $\lambda^2 << T^2 << A$ (p. 81)*

F = 1 = Geometry factor at normal incidence (p. 25-27)*

A = Surface Area (p. 78)*

$\nu_{xy}^2 = (k\psi)^2$ for small angles

Therefore the equation reduces to for small angles

$$\frac{I(\psi, \eta)}{I_0} = e^{-k^2\sigma^2} \left[\rho_0^2(\psi, \eta) + \frac{\pi T^2}{A} e^{-(k\psi T/2)^2} \right] \qquad (6)$$

Note that the subscript o refers to the quantities for a perfectly smooth surface.

*Refers to page numbers where definitions in Beckman and Spizzichino are found.

Some interesting results are that two terms, one for diffraction, and one for scattering occur. While the diffraction term is a function of ψ and η, the scattering term depends only on ψ. The intensity is reduced by a factor $e^{-k^2\sigma^2}$ by the randomness of the surface; however this is partially compensated for by the scatter term. Since $T^2 \ll A$ the scatter term is much smaller than the diffraction term at $\psi = 0$ but will predominate as ψ grows and the diffraction term diminishes. Note also that the scatter term grows as A decreases which is the same effect as seen for diffraction. Therefore as the cube corner is tilted we would expect a non-symmetrical spreading due to diffraction, plus a symmetrical spreading due to increased scatter.

The random errors in the dihedral angles cannot be taken into account by the above equation since they violate the condition that $T^2 \ll A$. However for an array of many cubes with random errors we would expect a Gaussian far field pattern if diffraction and scatter could be neglected.

6.0 EXPERIMENTAL POINT SPREAD FUNCTIONS

To this point our discussion has not led to a definite conclusion as to what point spread function we should expect. There is a strong tendency to expect a diffraction pattern, or a normal distribution due to random errors depending upon what magnitude of fabrication errors are assumed. However, tests have not shown this to be true. Rather an equation of the form

$$\frac{I(\psi, \eta)}{I(0, 0)} = e^{-c\psi/\gamma} \tag{7}$$

where

$$\gamma^2 = \frac{b^2}{1 - \epsilon^2 \cos^2 \eta}$$

and

$$\epsilon^2 = 1 - \left(\frac{b}{a}\right)^2$$

appears to provide the best fit to the data.*

*For planar arrays

This equation predicts a point spread function whose iso-intensity contours are ellipses with eccentricity ϵ.

If we let

$$P(\psi, \eta) = \frac{\sqrt{1 - \epsilon^2}\, c^2}{2\pi b^2}\, e^{-c\psi/\gamma} \tag{8}$$

Then it may be shown that

$$\int_0^{2\pi} \int_0^{\infty} \frac{\sqrt{1 - \epsilon^2}}{2\pi b^2}\, e^{-c\psi/\gamma}\, \psi d\psi d\eta = 1 \tag{9}$$

as required by conservation of energy. The ellipticity of the pattern is caused by the angle of incidence of the radiation at the cube corner. By our definition of terms the radiation is incident in the plane containing $\eta = \pi/2$ so that the long dimension of the intensity pattern will always be in the $\eta = \pi/2$ or $3\pi/2$ direction with

$$\epsilon = f(\theta_i) \tag{10}$$

where θ_i is the incidence angle. Substituting $\epsilon = 1.16\sqrt{\theta_i}$ gives a good fit over the range $\theta_i = 0$ to $\theta_i = \pi/4$ which includes most angles of interest. Therefore

$$P(\psi, \eta, \theta_i) = \frac{\sqrt{1 - 1.35\,\theta_i}}{2\pi b^2}\, e^{-c\psi/\gamma} \tag{11}$$

where

$$\gamma^2 = \frac{b^2}{1 - 1.35\,\theta_i \cos^2 \eta}$$

The value of c/b can be found by examining the point spread functions at normal incidence ($\theta_i = 0$). Since only the ratio c/b enters the equation it is not necessary to find them independently simplifying.

$$P(\psi, \eta, \theta_i) = \frac{\sqrt{1 - 1.35\,\theta_i}}{2\pi}\, p^2 e^{-\sqrt{1-1.35\,\theta_i \cos^2 \theta_n}\, p\psi} \tag{12}$$

where $p = c/b$

It should be noted that if the cube corner is not rotationally symmetric, the point spread function will depend upon the azimuth of incidence ϕ_i as well as θ_i. For the Hexagonal cube corners used on most satellites the minor variations due to ϕ_i are neglected.

Values of p for several satellite arrays determined by analysis of the far field intensity patterns are shown in Table 1.

7.0 THE VELOCITY ABERRATION

Up to this point the need for a two dimensional point spread function has not been made clear. The need arises because of the velocity aberration effect which is a function of orbital position and the direction of the velocity vector with respect to the transmitter/receiver axis. This effect causes the receiver to be located at various points in the far field pattern as a function of the orbit and velocity vector parameters.

If a satellite equipped with a cube corner array is moving with a velocity V' normal to the transmitter/satellite axis, a Bradley or velocity aberration effect causes the reflected beam pattern to be angularly displaced by an amount

$$\psi_V = \frac{2V'}{c} \tag{14}$$

where c is the speed of light. Therefore, the reflected radiation pattern is not centered on the transmitter, but is displaced by the angle ψ_V in the plane containing the velocity vector and the transmitter/satellite axis.

However, for a satellite in circular orbit, the velocity vector will only be normal to the transmitter/satellite axis when the satellite is at zenith. The more general case is shown in Figure 6. This figure shows the satellite at zenith angle θ, and altitude h. The satellite and transmitter are in the YZ plane with the transmitter located at the point (o, o, R_e) where R_e is the radius of the earth (6370 Km). For purposes of our calculation the earth will be assumed spherical and the orbit circular. The satellite is located at the position (o, msin θ_r, r cos θ_r). Under these conditions the slant range ρ is

$$\rho = r\nu - R_e \cos\theta \tag{15}$$

where

$\nu = \sqrt{1 - (R_e/r)^2 \sin^2 \theta}$
$r = R_e + h$
h = Satellite altitude
θ = Angle between z axis and slant range ρ

The angle between the slant range ρ and the radius r is denoted as γ and is equal to

$$\gamma = \frac{R_e}{r} \sin \theta \tag{16}$$

The orientation of the satellite reference system to the satellite/transmitter axis can be specified by a polar coordinate system centered around the ρ axis with ψ the angular distance from the axis and η its azimuth when viewed in the satellite transmitter direction. The zero reference for η will be selected as the -X direction. Therefore a gravity gradient satellite will have its gravity gradient axis oriented in the direction

$$\psi = \gamma$$

$$\eta = 3\pi/2$$

Azimuth angles are measured counterclockwise.

In order to define the velocity vector, we must establish its direction and magnitude. Since the vector is always in the plane normal to the radius r we need only specify its direction by an azimuth which we will call ω again referenced to the -X direction.

The velocity normal to the ρ axis is

$$V' = V\sqrt{\cos^2 \omega + \nu^2 \sin^2 \omega} \tag{16}$$

and its direction is

$$\eta = \tan^{-1} [\nu \tan \omega] \tag{17}$$

Two special cases are of interest. The first occurs when $\omega = 0$ or π. Under this condition

$$V' = V \quad \text{and} \quad \eta = 0 \tag{18}$$

This condition occurs at the highest point in a satellite pass and corresponds to the maximum velocity aberration. Note that maximum velocity aberration can occur at any zenith angle and that a pass through zenith is not required. The second case of interest occurs when $\omega = \pi/2$ or $3\pi/2$. When this occurs

$$V' = \nu V$$

For satellites in high orbits $\nu \approx 1$ and $V' \approx V$.

This indicates that for satellites in high orbits, the velocity aberration is nearly constant and independent of both ω and θ.

In contrast, for low orbiting satellites, the velocity V' can vary from V at zenith to nearly zero at the horizon.

The absolute value of velocity aberration is shown in Figure 7 as a function of satellite altitude. Data for this curve are shown in Table 2. The variation in velocity aberration with θ and ω is shown in Figure 8 for a 1000km orbit, while Table 3 provides values for several orbit heights.

8.0 EVALUATING CROSS SECTION

We now have all the equations necessary to calculate the effective cross section of a retrodirector array in orbit. The procedure is as follows. Using the data on effective area and point spread function, compute cross section using Equation 4. The result will be an expression involving four parameters.

$$\sigma = f(\theta_\ell, \phi_\ell, \psi, \eta) \tag{20}$$

Next, compute ϕ_ℓ from Equation 16 ($\theta_1 = \gamma$). If the cross section is a function of ϕ_ℓ compute ϕ_ℓ. For non-rotating satellites $\phi_\ell = \omega - \pi/2$. For rotating satellites a time function must be computed for relating ϕ_ℓ to ω. Using Equations 14, 16, and 17 compute ψ, and η. Substitute these values of the four parameters into Equation 20 to obtain the cross section. Note, that in order to

solve for σ we must have the altitude of the satellite, the zenith angle θ and the velocity vector azimuth ω as given data.

We now have obtained the cross section of the satellite as a function of its orbital position. However in order to use cross section we must apply the radar equation. Values of cross section are shown for most of the arrays in orbit in Table 5.

9.0 THE RADAR EQUATION

The classical radar equation is

$$S = \frac{E_T G_T G_R \lambda^2 \sigma}{(4\pi)^3 R^4} \tag{21}$$

where

S = Received signal Energy
E_T = Energy generated by transmitter
G_T = Antenna gain of transmitter optics
G_R = Antenna gain of receiver optics
λ = Wavelength
σ = Radar (lidar) cross section of target
R = Range of target*

In practical operational conditions a loss factor for the transmission of the receiver and transmitter optics τ_0 and a factor for atmospheric transmission τ_a must be included. Equation 21 becomes

$$S = \frac{E_T G_T G_R \lambda^2 \sigma \tau_0 \tau_a^2}{(4\pi)^3 R^4} \tag{22}$$

Of the parameters in Eq. 22 some are dependent upon the lidar system used, some depend upon the propagation path, and one depends upon the target. In practice, a critical value of S dependent upon the receiver system and noise sources determines the required value of the right hand side of equation 22.

$$S_c \leq \frac{E_T G_T G_R \lambda^2 \sigma \tau_0 \tau_a^2}{(4\pi)^3 R^4} \tag{23}$$

* ρ was used for target range in Section 7.

If we define three parameters as follows

$$P_s \equiv E_T G_T G_R \tau_0 \lambda^2 \quad \text{meters}^2 \equiv \text{Station Parameter}$$

$$P_p \equiv \frac{\tau_a^2}{(4\pi)^3 R^4} \quad \text{meters}^{-4} \equiv \text{Path Parameter}$$

$$P_T \equiv \sigma \quad \text{meters}^2 \equiv \text{Target Parameter}$$

then Eq. 23 simplifies to

$$P_s P_p P_T \geq 1 \tag{24}$$

The reason for defining the parameters in this manner is that each of these three parameters is normally under the control of a different group. The tracking station operators can control P_s but P_p is usually controlled by the orbital requirements of the spacecraft. The final parameter P_T or simply σ must be optimized by the cube corner array designer to make the triple product as large as possible but in any case greater than unity.

We will now analyze the three parameters.

The required signal S_c is determined by the number of photoelectrons detectable by the detector circuitry. This number N is presently set at about 100 but can vary depending upon ranging accuracy requirements and detector noise. Signal energy is related to N by the following relation

$$S_c = \frac{(h\nu)\, N}{\eta} \tag{25}$$

where

$h\nu$ = Energy of a photon
η = Detector quantum efficiency

For the most common lasers (Ruby and Doubled Nd - Yag)

$$S_c = \frac{(2.5 \times 10^{-19})\,100}{0.05} = 5 \times 10^{-16} \text{ Joules } (\lambda = 0.69 \times 10^{-6} \text{ m})$$

$$S_c = \frac{(3.8 \times 10^{-19})\,100}{0.20} = 1.9 \times 10^{-16} \text{ Joules } (\lambda = 0.53 \times 10^{-6} \text{ m})$$

The antenna gain is controlled by the $1/e^2$ power beamwidth desired (Assuming a Gaussian beam profile) by the following equation

$$G_T = 32/\theta_T^2 \tag{26}$$

Receiver gain may be obtained from the classical formula (D_r = receiver diameter)

$$G_R = \left[\frac{\pi D_r}{\lambda}\right]^2 \tag{27}$$

System losses τ_0 must be obtained by a careful analysis of the optical losses in the transmitter and receiver optics.

For the laser tracking stations presently in use by NASA/GSFC the value of the station parameter is

$$P_s = 5.11 \times 10^{22} \text{ meters}^2 = 227.1 \text{ dB meters}^2 \tag{28}$$

where the following station parameters were used

E_T = 1.0 Joules
θ_T = 5×10^{-4} radians
D_r = 0.51 meters
λ = 0.6943×10^{-6} meters
τ_0 = 0.078

The path parameter depends upon two variables, satellite altitude and zenith angle. For a circular orbit of altitude h

$$R = \sqrt{(R_e + h)^2 - (R_e \sin\theta)^2} - R_e \cos\theta \tag{29}$$

where R_e = Earths Radius = 6.37×10^6 m. The atmospheric transmission may be computed by the following relation

$$\tau_a = \tau_{a0}^{\sec\theta} \tag{30}$$

where τ_{a0} = zenith atmospheric transmission. Zenith atmospheric transmission ranges from 0.75 at 0.53×10^{-6} meters to 0.83 $\times 10^{-6}$ at 0.69×10^{-6} meters under clear sky conditions but can of course drop to nearly zero under poor visibility conditions. A value of 0.70 is normally used in calculations. The path parameter can easily be evaluated on a desk type computer. A solution for an orbital height of 1000 km is shown in Table 4.

Table 1
Values of the Constant p for NASA
Cube Corner Arrays

Satellite	p
BE-B	2.16×10^4
BE-C	2.16×10^4
GEOS-I	2.00×10^4
GEOS-II	4.55×10^4
GEOS-C	Not tested at writing date
Timation III	Data not reduced

Table 2
Maximum Velocity Aberration as a Function
of Orbital Altitude

Altitude (Km)	Velocity Aberration (Rad $\times 10^{-6}$)
0	53
500	51.3
1,000	49.5
2,000	46.4
4,000	41.7
8,000	35.4
16,000	28.4
32,000	21.7
64,000	16.0
128,000	11.6
256,000	8.29
512,000	5.90

Table 3
Variation of Apparent Velocity as a Function of Zenith Angle (θ)
and Velocity Vector (ω) for Several Altitudes

θ (Deg)	ω (Deg)	h = 0		h = 1000 Km		h = 10,000 Km	
		V'/V	η (Deg)	V'/V	η (Deg)	V'/V	η (Deg)
0	0	1.00	0	1.00	0	1.00	0
15	0	1.00	0	1.00	0	1.00	0
	45	0.98	44	0.99	44	0.99	45
	90	0.97	90	0.97	90	0.99	90
30	0	1.00	0	1.00	0	1.00	0
	45	0.94	41	0.95	42	0.99	45
	90	0.87	90	0.90	90	0.98	90
45	0	1.00	0	1.00	0	1.00	0
	45	0.87	35	0.90	38	0.98	44
	90	0.50	90	0.79	90	0.96	90
60	0	1.00	0	1.00	0	1.00	0
	45	0.79	27	0.85	34	0.97	43
	90	0.50	90	0.66	90	0.94	90
73	0	1.00	0	1.00	0	1.00	0
	45	0.73	15	0.81	29	0.96	43
	90	0.26	90	0.33	90	0.92	90

Table 4
Satellite Cross Section at Zenith

	Range ($m \times 10^6$)	Max Velocity Aberration (Rad $\times 10^{-6}$)	Effective Area* (cm^2)	p Value ($\times 10^4$)*	Gain (dB)	Cross Section ($m^2 \times 10^6$)**	Cross Section/(Range) 4
1. BE-B	1.13	49	142	2.16	85.1	4.60	2.82×10^{-18}
2. BE-C	1.00	49	142	2.16	85.1	4.60	4.60×10^{-18}
3. GEOS I (A)	1.95	46	1793	2.00	85.0	57.2	3.96×10^{-18}
4. GEOS II (B)	1.53	48	2147	4.55	86.7	100	18.2×10^{-18}
5. GEOS III (C)	0.93	50					
6. TIMATION III	14.0	29	540		92.8	103	1.62×10^{-2}
7. LAGEOS	5.90	38	257		86.0	10.8	8.91×10^{-21}
8. LUNAR ARRAYS	360	7.0	$\simeq$1000		96.0	400	2.4×10^{-26}
9. STARLET	0.92	50	101		77.4	0.55	7.67×10^{-19}

*Effective Area and p value are computed for the satellite at zenith. The p value is used to compute the gain function by the following relation

$$G(\psi) = 4\pi P(\psi) = \frac{4\pi}{2\pi} p^2 e^{-P\psi} = 2p^2 e^{-P\psi}$$

**At $\psi = \alpha_v$

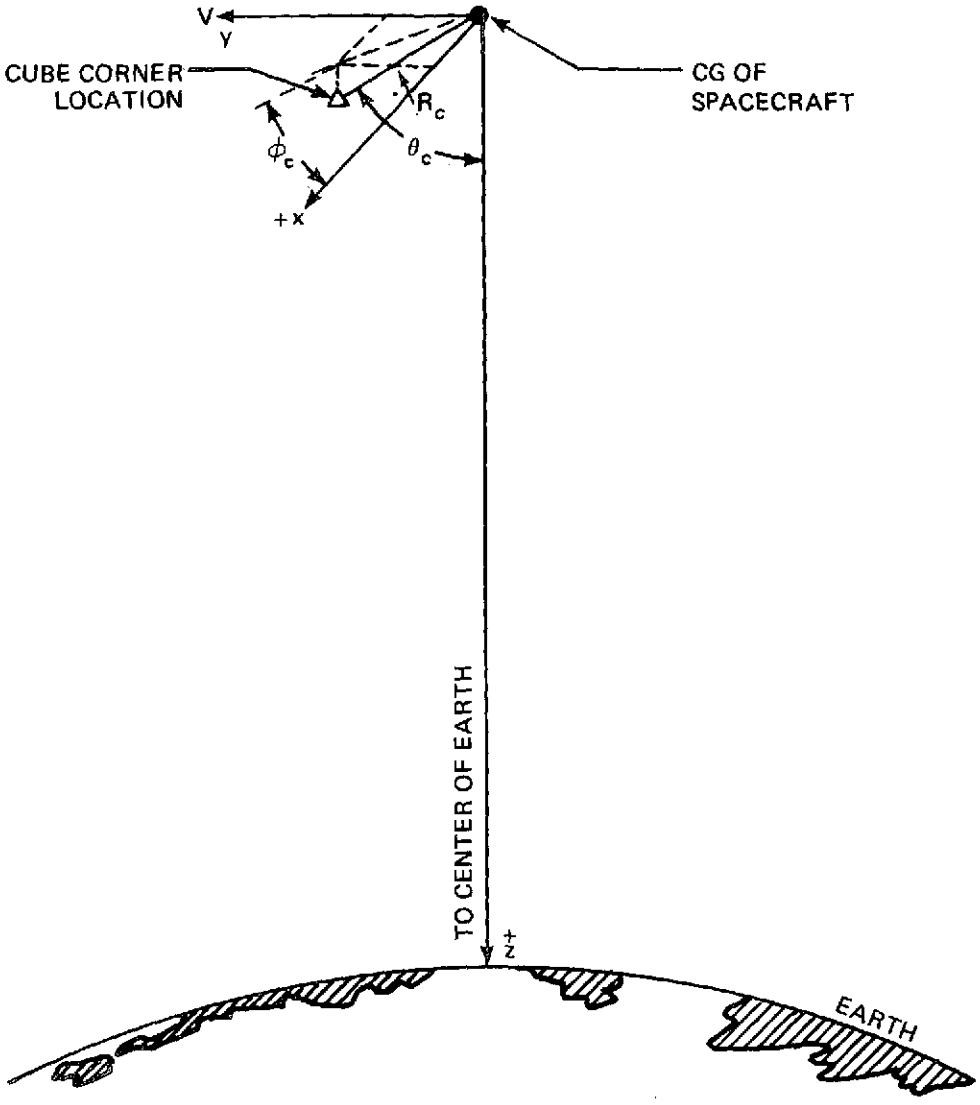
V
Y
CUBE CORNER
LOCATION
CG OF
SPACECRAFT
R_c
ϕ_c
θ_c
+x
TO CENTER OF EARTH
+
Z
EARTH

Figure 1.

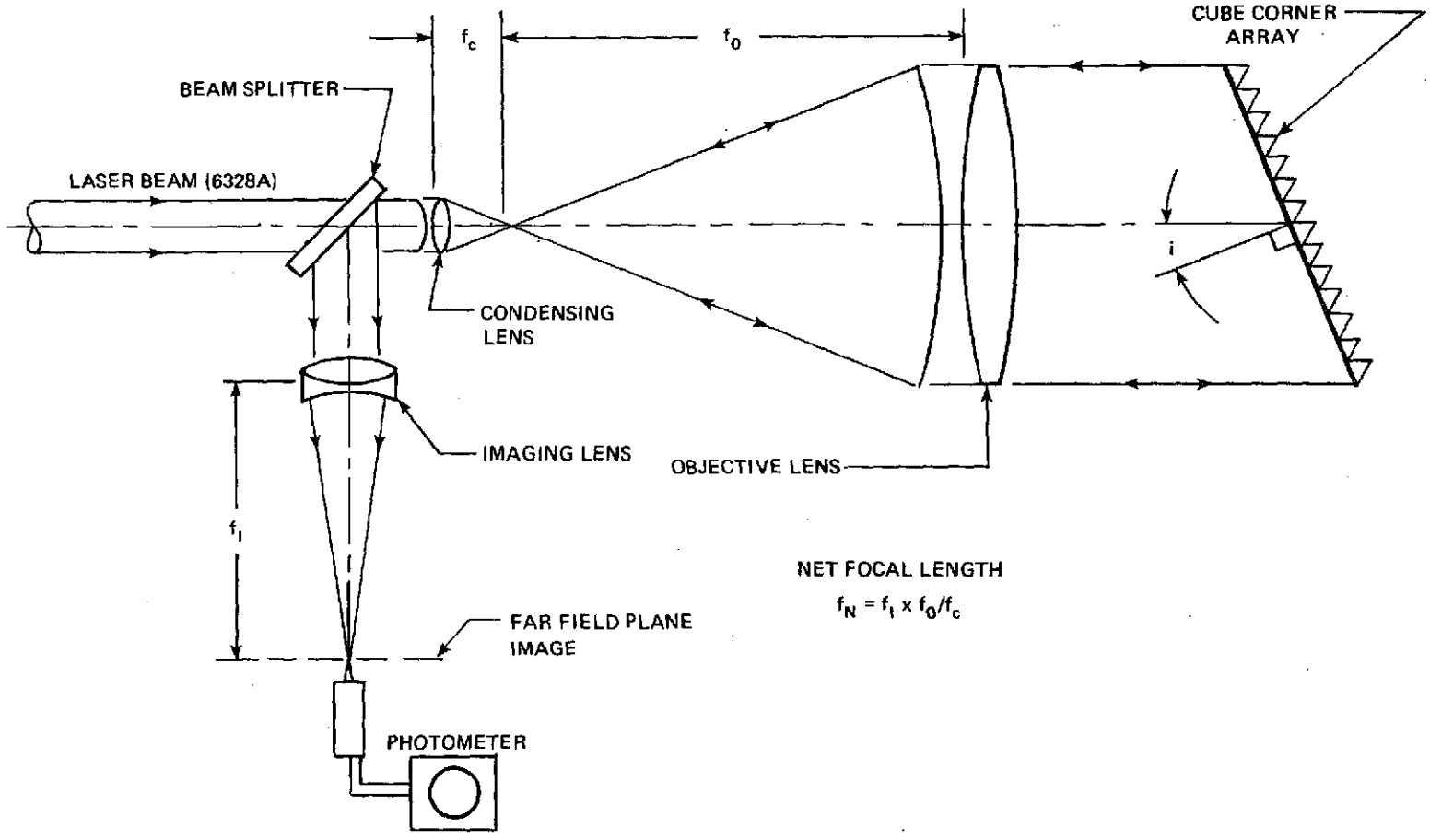

Figure 2a. Optical schematic of test setup for measuring cube array area.

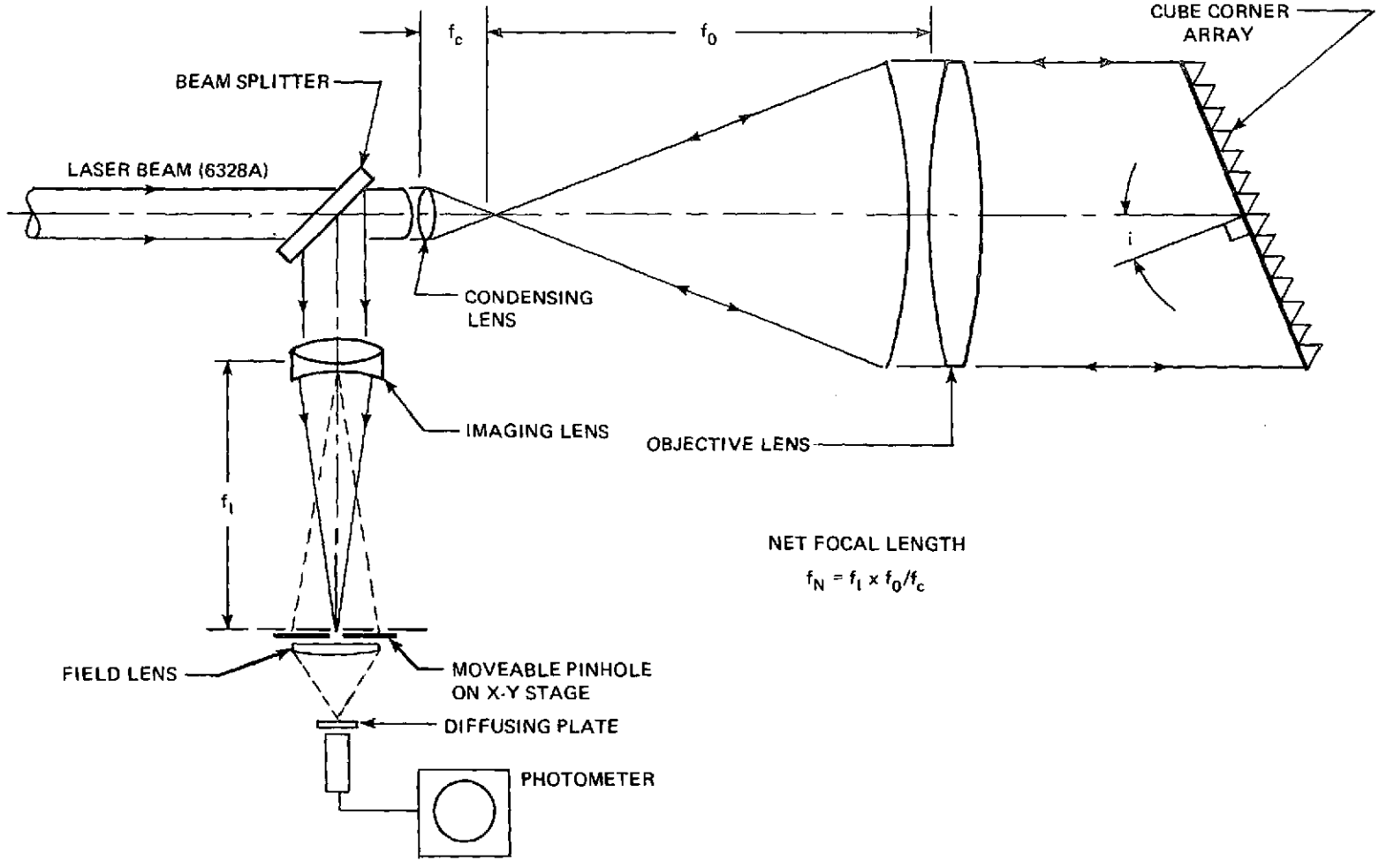

Figure 2b. Optical schematic of test setup for measuring point spread function.

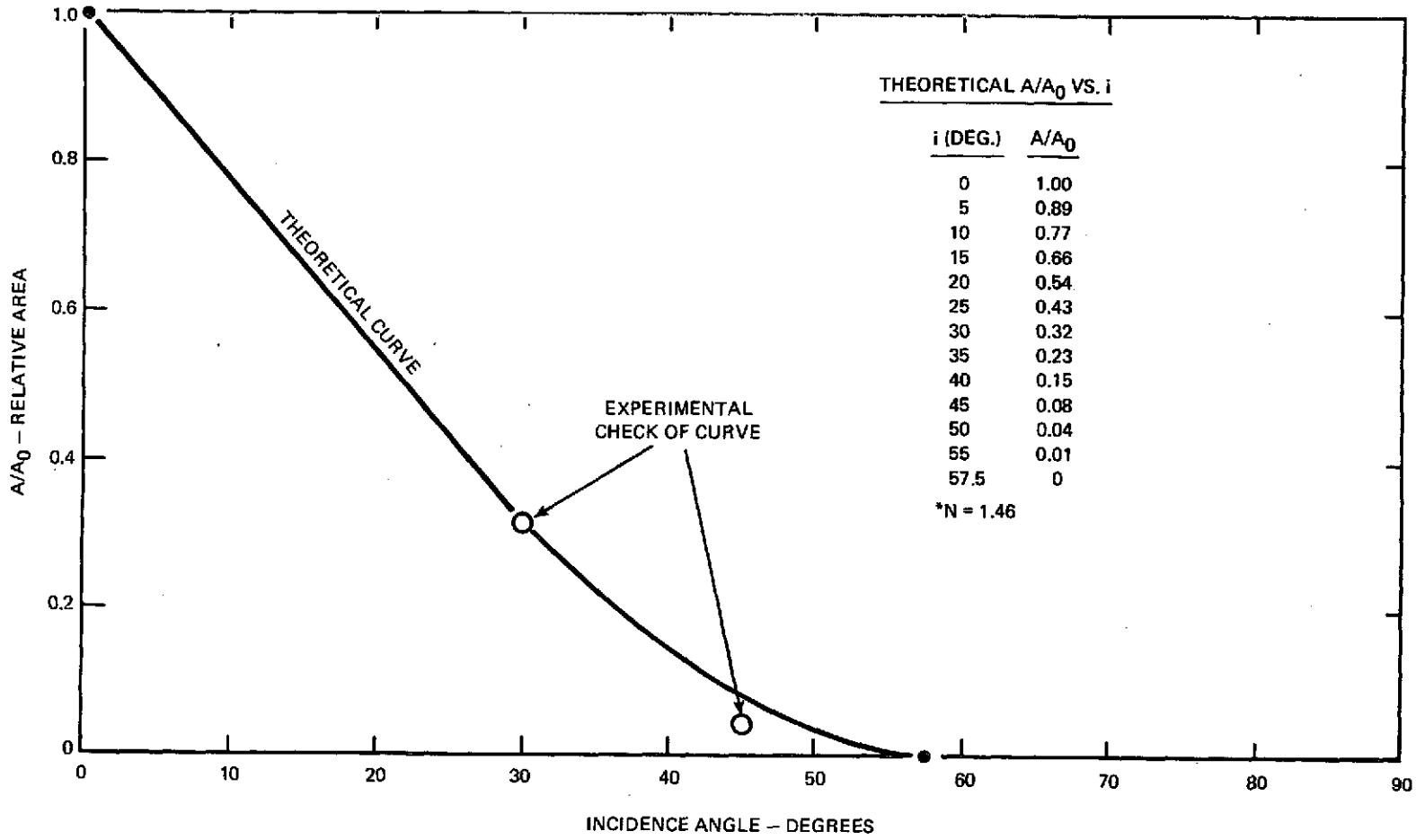

Figure 3. Relative area of GEOS A cube corner panels as a function of incidence angle.

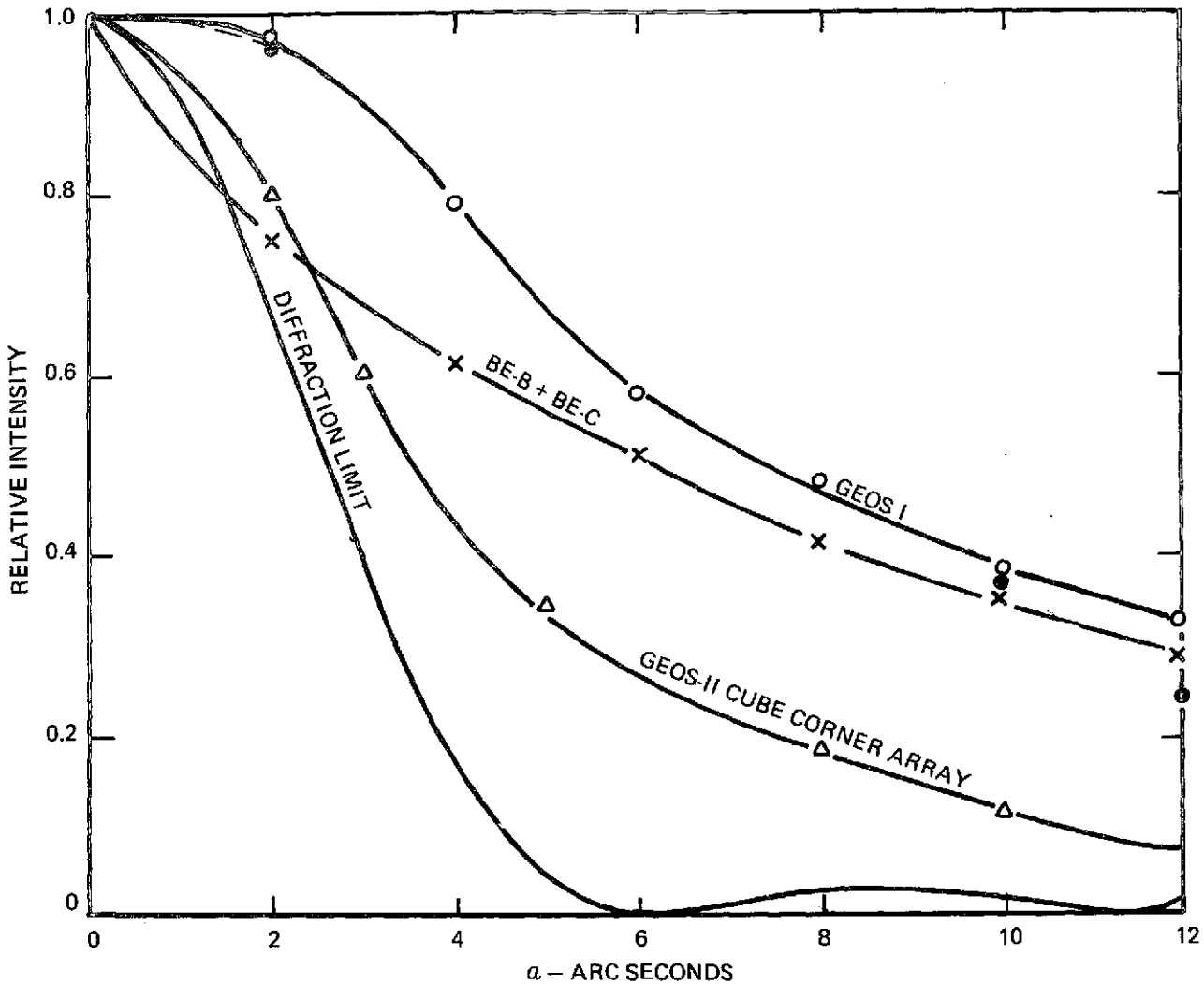

Figure 4. Far field patterns for cube corners used on several satellites*.

*ALL TESTS MADE AT NORMAL INCIDENCE
ALL CUBE CORNERS HAD 2.54 CM HEXAGONAL
ENTRANCE PUPILS

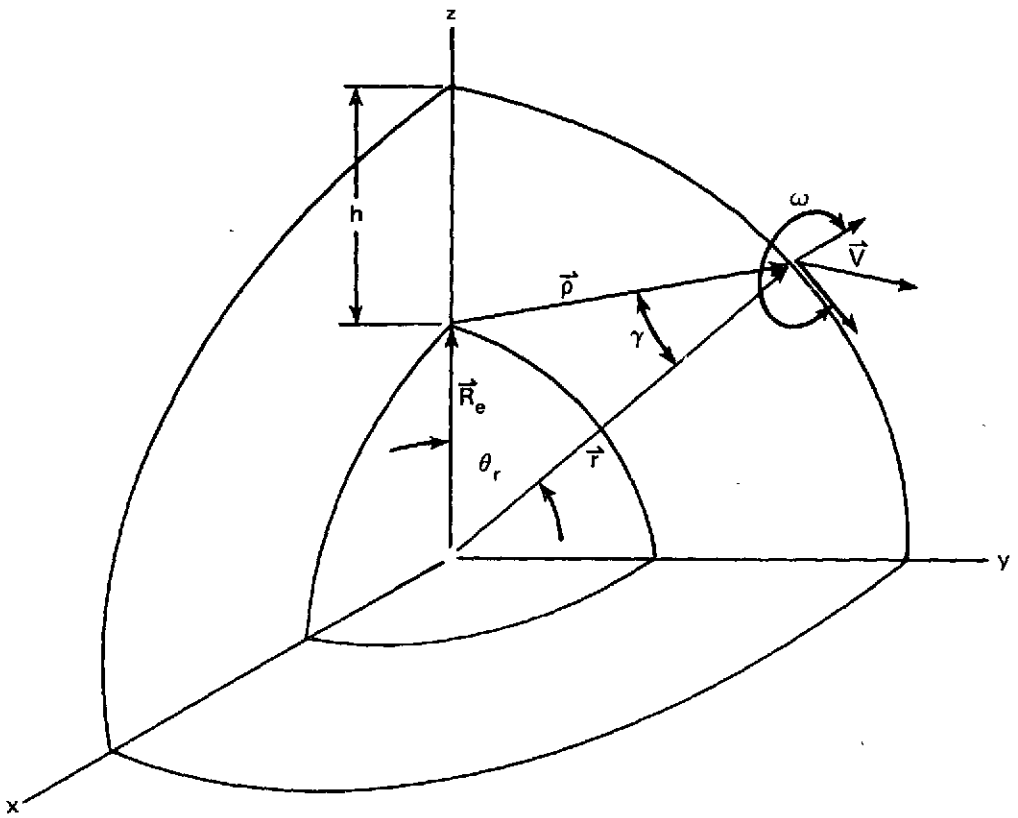

Figure 6. Definition of parameters used in calculation of velocity aberration.

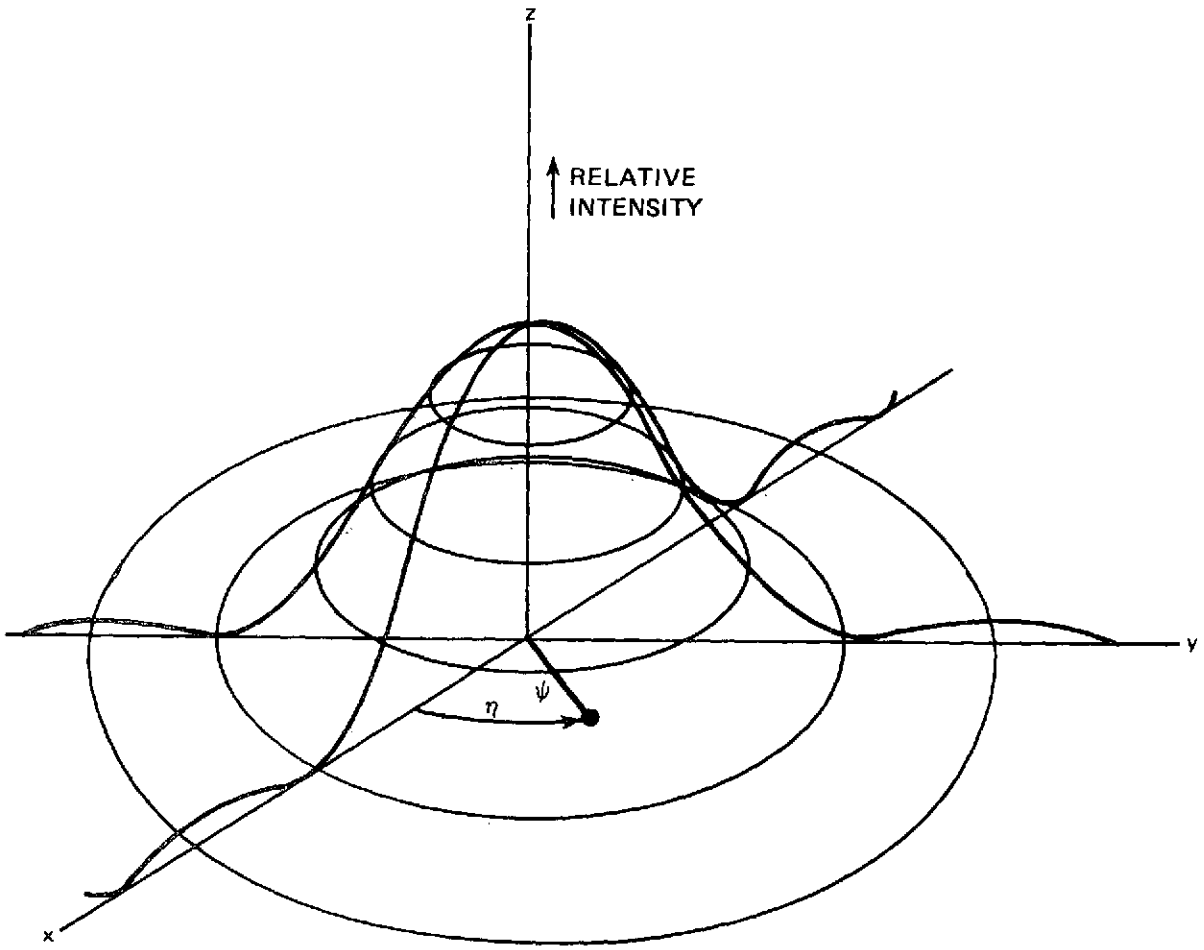

Figure 5. Coordinate system for far-field intensity pattern.

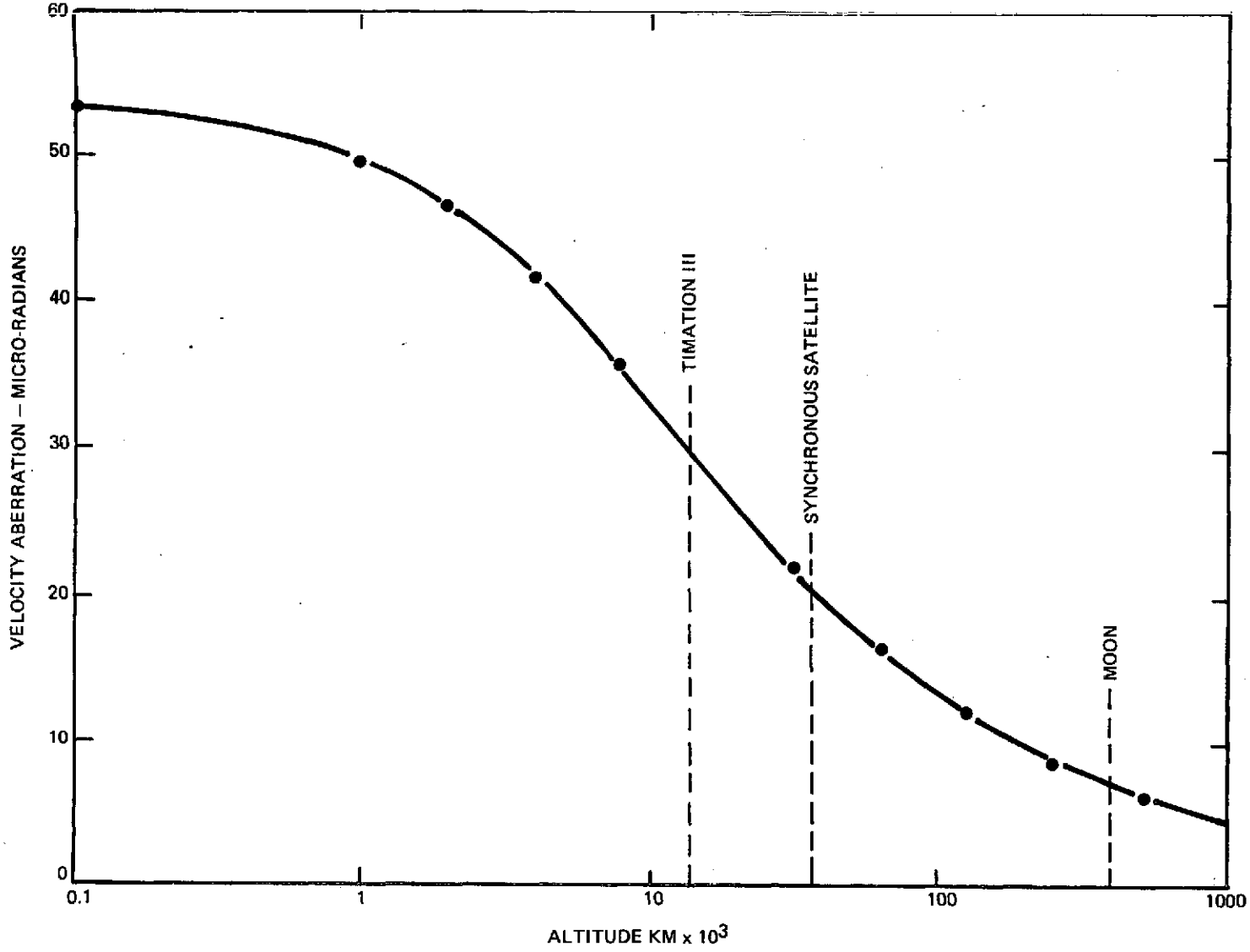

Figure 7. Maximum velocity aberration as a function of orbital altitude.

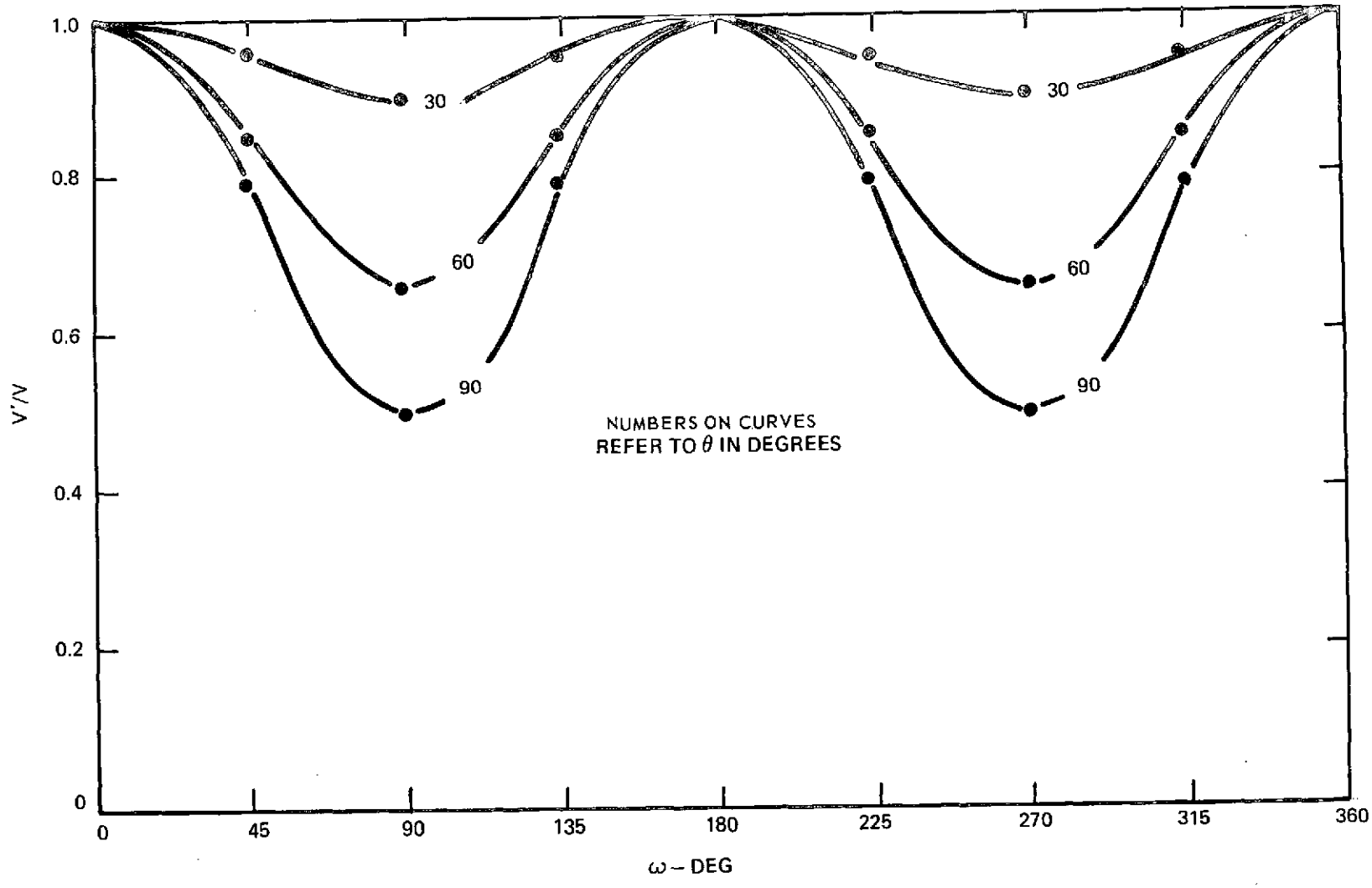

Figure 8. Variation of apparent velocity as a function of zenith angle (θ) and velocity vector angle (ω) for near earth satellite (h = 1000 km)